Theory of Multiple Exciton Effects in the Photosynthetic Antenna Complex LHC-II

Thomas Renger* and Volkhard May

Institut für Physik, Humboldt-Universität zu Berlin, Hausvogteiplatz 5−7, D-10117 Berlin, Germany

Received: October 29, 1996; In Final Form: April 8, 1997[⊗]

For an explanation of ultrafast spectroscopic data observed at the photosynthetic antenna complex LHC-II of higher plants, a density matrix theory is presented. It accounts for the dissipative exciton motion among the various chlorophyll molecules in the LHC-II and enables one to simulate the time-resolved pump−probe experiments of previous work in the literature. In order to model exciton annihilation effects appearing at higher pump−beam intensities, standard exciton theory is extended to the inclusion of a second higher excited singlet state and the internal conversion process from this state to the first excited singlet state. Concentrating on a heterodimer model of the LHC-II, the approach reproduces quite well the observed ultrafast pump−intensity dependent differential absorption.

1. Introduction

The theory of excitons in molecular crystals and aggregates which has been elaborated over some decades found its fascinating application in clarifying details of the functionality of the photosyntheticly active organism. In these biological systems light energy is used to realize a charge separation process which is the first step in synthesizing energetically reach chemical compounds. It is a well-established fact that after its absorption light energy moves via an exciton mechanism. Bacteria and higher plants collect light energy in the so-called antenna complexes formed by special chlorophyll (Chl) containing proteins.

The structure of some of these antenna complexes could be already resolved. Especially, the recent structure resolutions of the highly symmetrical bacterial antenna complex LH-II[2] gave remarkable stimulation both to experimentalists as well as theoreticians to achieve a deeper understanding of the structure function relationship in these systems. (This special issue demonstrates the efforts undertaken in this field.) With application of ultrafast spectroscopic techniques on antenna complexes with a known structure, the structure function relation can be clarified down to a sub-picosecond time scale (For a review on this topic see for instance ref 3). But, to get a clear interpretation of the measured data accompanying theoretical calculations is indispensable.

The present paper deals with such simulations but concentrates on pigment−protein monomers of the light harvesting complex LHC-II of higher plants. Recently it was possible to clarify the structure of this type of pigment−protein complex.[4] It contains 12 Chl molecules, among them 7 Chl*a* and 5 Chl*b* which are positioned one to another in a definite spatial arrangement. However, the mutual arrangement is not so regular as in the case of the LH-II. And, there are two different types of Chl's. But, the two types, the Chl*a* and Chl*b* molecules, form strongly correlated heterodimers distributed over the whole sectional view of the protein in the membrane.

In some foregoing papers[5−8] we already dealt with this type of pigment−protein complex. Especially, it was possible to demonstrate that the heterodimer model consisting of a pair of a Chl*a* and a Chl*b* molecule suffices to explain the subpicosecond part of the one- and two-color pump−probe experiments of ref 1. This success in our simulations mainly relies on the fact that excitation energy redistribution from the initially excited Chl*b* molecules appears in the first step to the nearest, and hence most strongly coupled, Chl*a* molecule. Redistribution over all other Chl*a* molecules takes place on a somewhat longer time scale (several picoseconds). In the present paper we proceed in dealing with the dimer model of the LHC-II. Of course, we will not take the position that such a restricted description would be sufficient in general. (First calculations for the whole complex are under way.)

For inclusion of irreversible excitation energy transfer from Chl*b* to Chl*a*, some mechanisms allowing for energy dissipation have to be incorporated into the theoretical description. These mechanisms are given by the vibrational modulation of the Chl excitation energy as well as by the modulation of the coupling among different Chl molecules. The respective vibrations may be intramolecular vibrations (high-frequency vibrations of the Chl skeleton) or those of the protein environment (low-frequency inter-molecular vibrations). It represents the standard in this field to account for all of these modes within a second-order perturbational treatment which only desires the knowledge of related vibrational spectral densities.[9−11,13] In contrast, a quantum dynamic description of a large set of vibrational modes is impossible. To overcome this difficulty, we introduced in ref 5 a model which splits off a single effective coordinate per Chl molecule from the continuum of the intra- and intermolecular vibrations. The dynamics of these coordinates are described quantum mechanically, and a coupling to the remaining modes (the reservoir modes) is also taken into account allowing for energy dissipation. Using an appropriate density matrix theory, vibrational coherences as well as their dephasing can be properly described. Since experimental data on vibrational coherences of photosynthetic antenna systems[14,15] and reaction centers[16,17] indicate vibrational periods of some hundreds of femtoseconds, the effective coordinates could be interpreted as special protein coordinates. For the present system the energy of the effective vibrational quanta can be estimated from the temperature dependence of the absorption and fluorescence line width.[18]

In extending these former calculations, we will demonstrate in the present paper how to model the pump−probe measurements of ref 1 in their dependence on the pump−beam intensity. It is well-accepted that the alteration of optical spectra with increasing pump intensity is originated by exciton−exciton annihilation (see, e.g., ref 3). If two excitons are excited simultaneously in the complex and they move close to one

[⊗] Abstract published in *Advance ACS Abstracts,* August 1, 1997.

S1089-5647(96)03372-X CCC: $14.00

another, it is possible that according to their mutual coupling one exciton recombines (from the first excited singlet state S_1 to the ground state S_0) and the other exciton jumps into a higher excited state. This process can be considered as a fusion of S_1 excitons. However, a fast nonradiative transition from the higher excited state to the S_1 state allows one exciton to be recreated. Such nonradiative transitions follow from internal conversion (IC) processes. In dye molecules like Chl these transitions from higher excited singlet states to the S_1 state are very fast (about 1 ps or less). We will include this process in our simulations and introduce a higher excited singlet state S_n ($n > 1$) of the Chl (ref 12), as well as a nonadiabatic coupling of this state to the S_1 state. In principle also the S_0 state is coupled nonadiabatically to the S_1 state as well as to the S_n state. However, the Chl S_1 state has a lifetime of some nanoseconds, and therefore the respective transition to the ground state does not occur on the ultrafast time scale we are interested in. The reason for this weak coupling is to find in the large energetic difference and the absence of other molecular states energetically between S_0 and S_1, whereas between S_1 and S_n there are many "bridge" states over which the excitation relaxes. With these considerations we are able to generalize the calculations of refs 19−22, where efficient schemes are offered to consider further excited singlet states for the exciton motion in an aggregate (e.g., the collective oscillator representation).

Our model as well as those of refs 19−22 includes the formation of multi-exciton states. However, in contrast to refs 19−22 with the application of $\chi^{(3)}$ theory, in the present contribution as in ref 7 the external light field will be incorporated exactly to allow for populations of higher exciton manifolds. Due to the exciton annihilation there is an irreversible relaxation between different exciton manifolds, which can alter the measured nonlinear optical response qualitatively as will be demonstrated later. In contrast to a perturbative treatment, the determination of a response function depending on multiple time arguments is circumvented in the present contribution.

The paper is organized as follows. In the next section we explain in detail a general aggregate model valid for any geometrical structure and any number of Chl molecules. It contains the coupling to intramolecular as well as intermolecular vibrations. Then, a density matrix theory is introduced which enables us to handle the two types of vibrational degrees of freedom in such a manner that the irreversible IC process as well as energy dissipation to protein vibrations is incorporated. The related reduced density matrix (RDM) not only describes the quantum motion of the excitons but also includes the effective protein coordinates. After a short explanation of how to calculate the time-resolved differential absorption, all results of our numerical calculations will be explained in section III. We offer an effective way to distinguish the different parts of the light-induced polarization and to propagate the huge number density matrix elements. Our model is succesfully applied to simulate the intensity dependent two-color pump−probe experiments of ref 1. Finally, some relationships of our nonperturbative approach to the standard treatment of nonlinear optics in a $\chi^{(3)}$ or $\chi^{(5)}$ scheme are offered.

II. Theory of Ultrafast Exciton Motion

A. The Model. We start with a general expression for a Chl aggregate Hamiltonian. It is appropriate to introduce a representation with respect to the electronic states $|jp\rangle$ of single molecule j with electronic quantum number p. The expansion basis should take into account the singlet ground state S_0, the first excited singlet state S_1, and a further excited singlet state S_n ($n > 1$). To have a short-hand notation, we write $p = g, e, f$ for the S_0, S_1, and S_n states, respectively. The complete Hamiltonian including the action of the external laser fields reads

$$H = \sum_j \Big(\sum_p (E_{jp} + H_{jp}(\mathbf{q}))|jp\rangle\langle jp| + [V_j|jf\rangle\langle je| + \mathrm{hc}]\Big) + \sum_{i>j} \hat{J}_{i,j} - E(\mathbf{r},t)\sum_j \hat{\mu}_j \quad (1)$$

The first contribution denotes the electronic excitation energy E_{jp} of electronic state p at molecule j combined with the related vibrational Hamiltonian $H_{jp}(\mathbf{q})$. All types of vibrational degrees of freedom (counted by the mode-index ξ), which are necessary in the theoretical description, have been condensed to $\mathbf{q} = \{q_\xi\}$. The nonadiabatic coupling V_j has been added to account for the IC processes from $|f\rangle$ to $|e\rangle$. The electronic interactions among different molecules i and j in the aggregate are described in the point dipole approximation according to the well-known formula

$$\hat{J}_{ij} = \frac{(\hat{\mu}_i \cdot \hat{\mu}_j)}{|\mathbf{R}_{ij}|^3} - \frac{3(\hat{\mu}_i \cdot \mathbf{R}_{ij})(\hat{\mu}_j \cdot \mathbf{R}_{ij})}{|\mathbf{R}_{ij}|^5} \quad (2)$$

The vector $\mathbf{R}_{ij}$ gives the center-of-mass distance between molecule i and j and the vectorial dipole operator of molecule j reads according to the three-level model (and neglecting a direct transition from $|g\rangle$ to $|f\rangle$)

$$\hat{\mu}_j = \mathbf{d}_j(f, e)|jf\rangle\langle je| + \mathbf{d}_j(e, g)|je\rangle\langle jg| + \mathrm{hc} \quad (3)$$

The dipole−dipole interaction covers three different types. The first part which is exclusively defined by the transition dipole moment of type $\mathbf{d}_j(e, g)$ describes the transfer of excitation energy among the first excited singlet states $|e\rangle$. Transfer of excitation energy between the states $|f\rangle$ and $|e\rangle$ is given by the term which only contains the transition dipole moments of the form $\mathbf{d}_j(f, e)$. Exciton fusion as the transformation of two states $|ie\rangle$ and $|je\rangle$ into the ground state and the state $|jf\rangle$ is related to the part proportional to both moments, $\mathbf{d}_i^*(e, g)$ and $\mathbf{d}_j(f, e)$. Followed by IC processes this gives a complete microscopic description of exciton−exciton annihilation. All values for the dipole−dipole coupling can be calculated since the spatial arrangement of the molecules in the LHC-II are known from ref 4 and values for the transition dipole moments $\mathbf{d}_j(e, g)$ are available. The second type $\mathbf{d}_j(f, e)$ of the dipole moments is not so precisely known. It enters our approach as a fit parameter $m = |\mathbf{d}_j(f, e)|/|\mathbf{d}_j(e, g)|$.

The last term in the Hamiltonian (1) describes the coupling to the radiation field. It takes into account the transition from the ground state to the first excited state, and furthermore the transition between $|e\rangle$ and $|f\rangle$. According to a pump−probe configuration, the total field strength splits off into the pump field with pulse envelope E_p and the probe (test) field with pulse envelope E_t

$$E(\mathbf{r}, t) = \sum_{\mathrm{s=p,t}} E_\mathrm{s}(t)\,(i\mathbf{k}_\mathrm{s}\mathbf{r} - i\Omega_\mathrm{s}t) + cc \quad (4)$$

Before explaining in detail the handling of the vibrational modes, we remind the reader about the relation of the model used to the standard Hamiltonian of exciton vibrational systems. To come into contact with the standard form of the exciton

vibrational Hamiltonian, one has to suppose parabolic potential energy surfaces (PES)

$$U_{jp}(\mathbf{q}) = U_{jp}^{(0)} + \sum_{\xi} \frac{\hbar\omega_{\xi}}{4}(q_{\xi} - q_{\xi}^{(jp)})^2 \tag{5}$$

We have used dimensionless coordinates of the various modes ξ with frequency ω_{ξ}. $q_{\xi}^{(jp)}$ defines the equilibrium position of coordinate q_{ξ} in the electronic state p at molecule j. The respective energy is given by $U_{jp}^{(0)}$. Calculating the bracket, one gets the potential energy of the vibrations

$$U_{vib}(\mathbf{q}) = \sum_{\xi} \frac{\hbar\omega_{\xi}}{4} q_{\xi}^2 \tag{6}$$

which is independent on the molecular state $|jp\rangle$. (Note the neglect of a change of the vibrational frequencies with changing molecular quantum numbers.) The mixed terms in eq 5 given by the product $q_{\xi}q_{\xi}^{(jp)}$ determine the electron (exciton) vibrational coupling

$$H_{\mathrm{ex-vib}} = -{}^1/_2 \sum_{jp}\sum_{\xi} \hbar\omega_{\xi} q_{\xi}^{(jp)} q_{\xi} |jp\rangle\langle jp| \tag{7}$$

This coupling type which is diagonal with respect to the electronic states can become off-diagonal after an expansion of the dipole−dipole coupling with respect to the vibrational coordinates q_{ξ}. Then, we may write

$$H_{\mathrm{ex-vib}} = \sum_{jp,j'p'}\sum_{\xi} \hbar\omega_{\xi} g_{\xi}(jp, j'p') q_{\xi} |jp\rangle\langle j'p'| \tag{8}$$

Within a density matrix description of exciton motion, relaxation among different excitonic states and related dephasing processes can be introduced by this general type of coupling (with dimensionless coupling constants $g_{\xi}(jp, j'p')$).

In contrast to this approach based on a perturbative consideration of the exciton vibrational coupling, we proceed in a way in which three separate subsets of the total set of vibrational modes **q** are introduced. (i) The first subset $\mathbf{Q} = \{\mathbf{Q}_j\}$ comprises the intramolecular vibrations $\mathbf{Q}_j$ of the j'th Chl molecule. They are of a high-frequency type and will be taken into account to provide resonance conditions for the excited state absorption and the IC process. (ii) The intermolecular vibrations resulting from the low-frequency motion of the protein environment define the second set **Z** of vibrational coordinates. They are responsible for energy dissipation and form a broad density of states. (iii) There exist a number of different experimental hints that coherent vibrational motion of the protein appears on a subpicosecond time scale. To take into account such vibrational coherences, we split off a single effective protein coordinate X_j per Chl. Introducing a coupling of these effective modes to the remaining set of protein vibrations energy exchange becomes possible. This remaining set of protein coordinates **Z** will be handled as a heat reservoir.

According to such a separation we provide the following type of vibrational Hamiltonian

$$H_{jp}(\mathbf{q}) = H_{jp}(X_j) + H_{jp}(\mathbf{Q}_j) + H(\mathbf{Z}) + K_{jp}(\mathbf{Q}_j, X_j, \mathbf{Z}) \tag{9}$$

(In order to avoid an extensive introduction of indices, every Hamiltonian is only specified by its dependence on particular vibrational coordinates.) The first two contributions describe the state-dependent motion of the single effective intermolecular coordinate X_j and of the set of intramolecular coordinates $\mathbf{Q}_j$ of molecule j, respectively. The Hamiltonian $H(\mathbf{Z})$ of the low-frequency protein vibration has been taken independently of the molecular states $|jp\rangle$. The coupling among all types of vibrational modes is contained in the fourth term of eq 9.

Having in mind the above introduced separation of the vibrational modes, we write the total Hamiltonian eq 1 as follows

$$H = H_{\mathrm{S}} + H_{\mathrm{S-R}} + H_{\mathrm{R}} \tag{10}$$

This separation into a system part H_{S}, a reservoir part H_{R}, and the coupling $H_{\mathrm{S-R}}$ among both is appropriate for the further description of the exciton dynamics by a properly defined RDM.

The Hamiltonian of the *relevant* system H_{S}, contained in eq 10, reads

$$H_{\mathrm{S}} = \sum_{j}\sum_{p} (E_{jp} + H_{jp}(X_j))|jp\rangle\langle jp| + \sum_{i>j} \hat{J}_{ij} - E(t)\sum_{j} \hat{\mu}_j \tag{11}$$

Any dependence of the two types of transition dipole moments and the three types of dipole−dipole coupling on the vibrational degrees of freedom has been neglected (Condon approximation). The incorporation of the effective modes X_j indicate that their quantum motion should be considered in an exact manner.

For the *system−reservoir* coupling we get

$$H_{\mathrm{S-R}} = \sum_{j}\Big(\sum_{p} K_{jp}(\mathbf{Q}_j, X_j, \mathbf{Z})|jp\rangle\langle jp| + [V_j|jf\rangle\langle je| + \mathrm{hc}]\Big) \tag{12}$$

Such an expression provides a model in which electronic energy dissipation is described by a coupling to the protein coordinates and an IC process.

Finally, the reservoir part of eq 1 reads

$$H_{\mathrm{R}} = \sum_{jp} H_{jp}(\mathbf{Q}_j)|jp\rangle\langle jp| + H(\mathbf{Z}) \tag{13}$$

It is formed by the intramolecular vibrations and the protein vibrations. Note, the electronic state dependence of the first part of H_{R} requires a slight modification of standard density matrix theory.

B. Density Matrix Theory. According to the general separation achieved in eq 10, we will utilize the standard technique of dissipative quantum dynamics resulting in the so-called *quantum master equation* for an appropriately defined RDM.[23] This type of equation considers the dynamics of the relevant system under the action of the reservoir degrees of freedom which remain in thermal equilibrium. The respective coupling between the system of interest and its surrounding, the reservoir, has been accounted for in a second-order perturbative treatment.

In the present case where two types of reservoirs appear we formulate the whole theory in the state representation from the very beginning.[23] This treatment is necessary to account for the electronic state dependence of the vibrational Hamiltonian $H_{jp}(\mathbf{Q}_j)$ (see eq 13).

We start by defining states of the complete system including the relevant system part and the reservoir. Since such states should characterize the total electron configuration of the aggregate, we may choose the *eigenstates* of H_{S}, eq 11 (at $\mathbf{E} = 0$). The definition of these states includes the dipole−dipole coupling. Therefore, they give (possibly delocalized) multiexciton states of the aggregate. Alternatively, one can choose the states obtained by neglecting the dipole−dipole coupling. We

will follow this line and take the electronic aggregate product states

$$|\mathbf{p}\rangle = \prod_j |jp\rangle \tag{14}$$

The multiindex **p** comprises the electronic quantum numbers p of every molecule j in the aggregate. Introducing the vibrational states related to the effective coordinates X_j according to

$$H_{jp}(X_j)|jpM_j\rangle = \epsilon(jpM_j)|jpM_j> \tag{15}$$

the vibrational state of all molecules reads

$$|\mathbf{p}M\rangle = \prod_j |jpM_j\rangle \tag{16}$$

The basis defined in the space of the relevant system may be shortened as

$$|a\rangle = |\mathbf{p}\rangle\ |\mathbf{p}M\rangle \equiv \prod_j |(|jp\rangle\ |jpM_j\rangle) \tag{17}$$

The reservoir states are defined in a similar manner. For those of the protein vibrations with the set of coordinates **Z** we write

$$H(\mathbf{Z})|\bar{\mu}\rangle = \epsilon(\bar{\mu})|\bar{\mu}\rangle \tag{18}$$

Here and in the following all eigenvalues of the various vibrational Hamiltonian are only distinguished by their particular quantum number.

For the states of the intramolecular vibrations we write

$$(\sum_{jp} H_{jp}(\mathbf{Q}_j)|jp\rangle\langle jp|)|a\mu\rangle = \epsilon(\mu)|a\mu\rangle \tag{19}$$

Note

$$|a\mu\rangle = \prod_j |jpM_j\,\mu_j\rangle \tag{20}$$

μ and $\bar{\mu}$ comprise the whole set of intra- and intermolecular vibrational quantum numbers, respectively. $H_{jp}(\mathbf{Q}_j)$ has been introduced in eq 9 and counts the intramolecular vibrational energy of molecule j starting at the energy $E_{jp} + \epsilon(jpM_j)$ (see eq 15). Additionally, the intramolecular states have to be characterized by the set of quantum numbers a of the relevant system. The energies $\epsilon(\mu)$ are independent of the quantum number a of the relevant system state (see also the reasoning in ref 23); i.e., we assumed that the intramolecular vibrational frequencies are the same in each electronic state. Now, a complete basis valid in the state space of the total system can be given

$$|\alpha\rangle = |a\rangle\ |a\mu\rangle\ |\bar{\mu}\rangle \tag{21}$$

Expanding the non-equilibrium statistical operator with respect to this basis

$$\hat{W}(t) = \sum_{\alpha\beta} \rho(\alpha|\beta;\, t)|\alpha\rangle\langle\beta| \tag{22}$$

the density matrix $\rho(\alpha|\beta;\, t)$ is obtained. The density matrix reduced to the states $|a\rangle$ of the system of interest follows as

$$\rho_{ab}(t) = \sum_{\mu\bar{\mu}} \rho(a\mu\bar{\mu}|b\mu\bar{\mu};t) \tag{23}$$

An equation of motion for this RDM will be derived according to the procedure of ref 23 by introducing the projection operator P which acts on an arbitrary matrix as

$$PA(\alpha|\beta) = \delta_{\mu,\nu} f(\mu)\delta_{\bar{\mu},\bar{\nu}}\, f(\bar{\mu}) \sum_{\kappa\bar{\kappa}} A(a\kappa\bar{\kappa}|b\kappa\bar{\kappa}) \tag{24}$$

The expression includes the thermal distributions $f(\mu)$ and $f(\bar{\mu})$ related to the intramolecular vibrations and the protein vibrations, respectively.

Starting with the equation of motion for the full density matrix $\rho(\alpha|\beta;\, t)$, one can derive an equation of motion for the RDM. All details of this derivation can be found in ref 23. We only quote here the result forming the basis of all further numerical studies. The equation of motion for the RDM introduced in eq 23 reads

$$\frac{\partial}{\partial t}\rho_{ab}(t) = -i\omega_{ab}\rho_{ab}(t) - i\sum_c (w_{ac}(t)\,\rho_{cb}(t) - w_{cb}(t)\,\rho_{ac}(t)) - \sum_{c,d} (\Gamma_{bddc}\rho_{ac} + \Gamma_{addc}\rho_{cb} - \{\Gamma_{cabd} + \Gamma_{dbac}\}\rho_{cd}) \tag{25}$$

In the following, the different parts of this equation are explained step by step.

The quantities $\omega_{ab} = (\epsilon_a - \epsilon_b)/\hbar$ are the transition frequencies in the spectrum of the relevant system states ($\epsilon_a = \sum_j \epsilon(jpM_j)$. The time-dependent coupling matrix elements w_{ab} are defined by the dipole−dipole coupling and the interaction term with the radiation field, both of which have been neglected in defining the system states $|a\rangle$. The matrix elements are obtained in taking the basic equation of motion for $\rho(\alpha|\beta;\, t)$ and, afterwards, reducing this equation to an equation for the RDM. We have to take the trace with respect to the reservoir states and get

$$\left(\frac{\partial \rho_{ab}}{\partial t}\right)_{|\text{dipole}} = \sum_{\mu\bar{\mu}}\sum_{\beta} (\langle a\mu\bar{\mu}|\sum_{i>j}\hat{J}_{ij} - \mathbf{E}(t)\sum_j \hat{\mu}_j|\beta\rangle\ \rho(\beta|b\mu\bar{\mu};t) - \langle\beta|\sum_{i>j}\hat{J}_{ij} - \mathbf{E}(t)\sum_j \hat{\mu}_j|b\mu\bar{\mu}\rangle\rho(a\mu\bar{\mu}|\beta;t) \tag{26}$$

Since we neglect any rearrangement of the protein coordinates **Z** upon electronic excitation, the summation with respect to the vibrational quantum numbers $\bar{\mu}$ can be simply carried out. The summation with respect to the quantum numbers μ of the intramolecular vibrations $\mathbf{Q}_j$ of the various molecules will be handled as follows. Noting expression 26, we see that there appear matrix elements of the type $\langle a\mu|\sum_{i>j}\hat{J}_{ij} - \mathbf{E}(t)\sum_j\hat{\mu}_j|b\nu\rangle$. Instead of taking into account all of these different types of matrix elements defined by the quantum numbers μ, we introduce single matrix elements of the dipole−dipole coupling and the coupling to the radiation field which includes effective transition dipole moments. For example, the matrix element $\langle jgM_j\mu_j|\mathbf{d}_j(eg)|jgN_j\nu_j\rangle$ (see the state definition in eq 19) is replaced by an effective matrix element $\mathbf{d}_j^{(eff)}(eg)$ and the Franck−Condon overlap integral of the vibrational states of the coordinates X_j. The effective matrix element should be related to a vertical transition in the scheme of the two respective PES defined by the intramolecular vibrations. Thus, it implicitly contains the Franck−Condon factor for such a vertical transition. The precise numerical value will be not calculated but determined by fitting the effective transition dipole matrix elements to experimental data (see below). Carrying out this procedure for every type of dipole moment, we get the time-dependent matrix elements in eq 25 as matrix elements taken with the states

$|a\rangle$ of the relevant system but including effective Franck−Condon renormalized transition dipole matrix elements

$$w_{ab}(t) = \langle a|\sum_{i>j}\hat{J}_{ij}^{(\mathrm{eff})} - \mathbf{E}(t)\mathrm{j}\sum_{j}\hat{\mu}_{j}^{(\mathrm{eff})}|b\rangle \qquad (27)$$

In the final part of explaining the various contributions to the RDM equation (25), we consider the dissipative contributions comprised in the relaxation matrices Γ_{abcd}. It is worth mentioning that the structure of the dissipative terms used provides the application of a Markov approximation. This might be questionable with respect to the considered time scale. Nevertheless, we apply this approximation (see also the discussion below).

In contrast to the exact consideration of the terms depending on the transition dipole moments, the dissipative contributions follow from a second-order perturbation theory with respect to the system−reservoir coupling eq 12. To clarify the structure of the relaxation matrix Γ, we first introduce the state representation of the system−reservoir coupling eq 12

$$\hbar\Theta(\alpha|\beta) = \langle\alpha|H_{\mathrm{S-R}}|\beta\rangle \qquad (28)$$

Then, we can directly follow our former derivations in ref 23 to get an expression for the relaxation matrix which governs the dissipative part of the RDM equation (25). It reads

$$\Gamma_{abcd}(\omega_{ab}) = Re\int_0^\infty \mathrm{d}t\ \mathrm{e}^{i\omega_{ab}t}\langle\Theta_{ab}(t)\ \Theta_{cd}(0)\rangle \qquad (29)$$

According to the second-order perturbational treatment, the expression contains the first and second moment of the coupling matrix Θ averaged with respect to the two types of reservoir states. Since the system−reservoir coupling eq 12 splits off into two separate contributions, the same is valid for the two types of moments. It has been explained in ref 23 that the first moment of the coupling Hamiltonian between modes X_j and $\mathbf{Z}$ vanishes identically (if a bilinear type of coupling has been chosen). Instead, a nonzero IC contribution remains. It would describe coherent motions between the states $|f\rangle$ and $|e\rangle$ (with a coupling constant V_j reduced by a Huang−Rhys type prefactor). The amplitudes of these oscillations, however, are negligible because of the large energetic difference between the states $|f\rangle$ and $|e\rangle$ (no emission or absorption processes of vibrational quanta are involved because the first moment gives only transitions between the same vibrational states). We concentrate on the irreversible part of the IC process and neglect respective first moments. (This has already been done in eq 25.) For the second moment we get

$$\langle\Theta_{ab}(t)\ \Theta_{cd}(0)\rangle = \sum_{\mu\bar{\mu}}\sum_{\nu\bar{\nu}} f(\mu)\ f(\bar{\mu})\ \exp(i\omega(\mu\bar{\mu};\nu\bar{\nu})t) \times \Theta(a\mu\bar{\mu}|b\nu\bar{\nu})\ \Theta(c\nu\bar{\nu}|d\mu\bar{\mu}) \qquad (30)$$

The transition frequencies introduced in eq 30 read

$$\omega(\mu\bar{\mu};\nu\bar{\nu}) = \frac{1}{\hbar}(\epsilon(\mu) + \epsilon(\bar{\mu}) - \epsilon(\nu) - \epsilon(\bar{\nu})) \qquad (31)$$

The part of the relaxation matrix Γ resulting from the coupling between the effective coordinates X_j and the reservoir of the remaining protein vibrations $\mathbf{Z}$ has been discussed at length for the case of a molecular dimer in refs 5 and 7. As in this foregoing paper, we take here a bilinear expression of the type $\sum_{jp\xi}K_{jp\xi}X_jZ_\xi$ and can directly apply former results. Before concentrating on the second contribution stemming from the IC process (the mixed contribution can be neglected[23]), we note that the general rate k_{ab} for a transition from state $|a\rangle$ to state $|b\rangle$ can be derived from eq 29 as $2\Gamma_{abba}(\omega_{ab})$. In the case of the IC process we get

$$k_{ab}^{(\mathrm{IC})} = 2\Gamma_{abba}^{(\mathrm{IC})}(\omega_{ab}) = \sum_j(\prod_{i\neq j}\delta_{p_i,q_i}\delta_{M_i,N_i})(\delta_{p_j,f}\delta_{q_j,e} + \delta_{p_j,e}\delta_{q_j,f})|\langle jp_jM_j|jq_jN_j\rangle|^2k_j^{(\mathrm{IC})}(p_j,q_j) \qquad (32)$$

This expression contains the IC rate for a transition between the electronic states p_j and q_j of molecule j (its dependence on M_j has been not explicitly indicated).

$$k_j^{(\mathrm{IC})}(p_j, q_j) = 2|V_j|^2Re\int_0^\infty \mathrm{d}t\sum_{\mu_j} f(\mu_j) \times \langle jp_jM_j\mu_j|e^{\mathrm{i}H_jp_jt/\hbar}\ \mathrm{e}^{-iH_{jq}jt/\hbar}|jp_jM_j\mu_j\rangle \qquad (33)$$

According to the choice of the electronic quantum numbers, this single-molecule rate may describe the transition from electronic state $|f\rangle$ to $|e\rangle$ as well as the reverse process. But the energetic distance between these states in relation to k_BT allows one to neglect the reverse process in the course of the numerical calculations.

Since the density matrix theory has been formulated in the representation of the electronic aggregate configurations together with the states of the effective modes X_j (compare eq 14 up to eq 17), the general rate eq 32 contains additional contributions. It takes notice of the electronic state of all other molecules of the aggregate which are not involved in the IC process. And, a Franck−Condon factor $\langle jp_jM_j|jq_jN_j\rangle$ appears which accounts for the overlap of the vibrational states related to the effective coordinates X_j before and after the IC process.

Although equations of motions for the type of RDM introduced in eq 23 could be derived independently of any concrete aggregate structure and the number of molecules involved, the possible numerical treatment strongly depends on the extension of the aggregate. Particularly, the inclusion of the effective vibrational coordinates X_j enlarges the numerical effort considerably. Therefore, it is reasonable to consider in the following the first nontrivial case which is given by a molecular dimer. Such an approach is corroborated by the known LHC-II structure with strongly correlated pairs of Chl*a* and Chl*b* molecules. Hence, in the case of a molecular dimer, we can write the states of the relevant system as $|1p\rangle\ |1pM\rangle\ |2q\rangle\ |2qN\rangle$. The two molecules have been labeled by 1 and 2 with electronic quantum numbers p and q, respectively. Therefore, nine different electronic configurations exist. The inclusion of the states related to the two effective coordinates X_1 and X_2 further enlarges the dimension of the state space (compare Figure 1). However, in the foregoing papers[5,7] it could be demonstrated that the dissipative motion within such a type of electron vibrational spectrum can be described. Here, only a further excited electronic state has been added.

C. Simulation of Pump−Probe Experiments. First we will give a brief summary of the standard theory of nonlinear optical response (see for instance ref 13). After this we want to go a little more into the details of the expansion of the density matrix with respect to the carrier waves of the applied laser beams (plane wave expansion). This approach is the key for managing the huge numerical effort connected with the consideration of two vibrational degrees of freedom X_j and the nonperturbative inclusion of the external pump field.

The optical response of the medium is determined by the induced polarization $P(\mathbf{r},t)$, which is obtained from the expectation value of the system dipole operator $\hat{\mu}$. Due to the nonlinear interaction with the strong pump field, the induced polarization

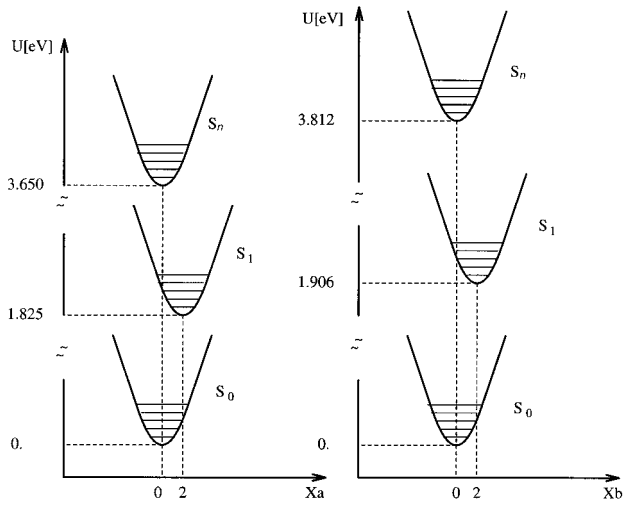

Figure 1. Potential energy surfaces of the Chl*a*−Chl*b* heterodimer model with the two effective coordinates X_a and X_b used in a dimensionless form.

wave will contain higher harmonics of the external field; i.e., it can be expanded as

$$P(\mathbf{r}, t) = \sum_{n_p,n_t=-\infty}^{+\infty} P_{n_p,n_t}(t)\, e^{i\sum_{s=p,t} n_s(\mathbf{k}_s\mathbf{r}-\Omega_s t)} \tag{34}$$

We will assume an optically thin sample and take notice of the envelope of the probe pulse which slowly varies in comparison to the optical frequency. Then, the time integrated absorption signal of the test- pulse is given by[13]

$$S_{tot.} = 2\Omega_t \int_{-\infty}^{+\infty} dt\, \mathrm{Im}\{E_t^*(t)\, P_{0,1}(t)\} \tag{35}$$

Besides the envelope of the probe field, also the envelope of the polarization traveling in the probe pulse direction enters ($\mathbf{k} = n_p\mathbf{k}_p + n_t\mathbf{k}_t$, $n_p = 0$, $n_t = 1$). To extract this particular contribution from the overall polarization, we introduce a similar expansion for the RDM at aggregate position **r**; i.e.,

$$\rho_{ab}(\mathbf{r},t) = \sum_{n_p,n_t=-\infty}^{+\infty} \rho_{ab}^{(n_p,n_t)}(t)\, e^{i\sum_{s=p,t} n_s(\mathbf{k}_s\mathbf{r}-\Omega_s t)} \tag{36}$$

The desired envelope of the polarization is then obtained as $P_{0,1}(t) = \sum_{ab}\langle a|\sum_j \hat{\mu}_j|b\rangle\rho_{ba}^{(01)}(t)$. Starting from the *quantum master equation* for $\rho_{ab}(\mathbf{r}, t)$ (eq 25) equations of motion for the various expansion coefficients $\rho_{ab}^{(n_p,n_t)}(t)$ are obtained in a straightforward manner

$$\begin{aligned}\frac{\partial}{\partial t}\rho_{ab}^{(n_p,n_t)}(t) = &-i(\omega_{ab} - n_p\Omega_p - n_t\Omega_t)\rho_{ab}^{(n_p,n_t)}(t) - \\ &i\sum_c(\langle a|\sum_{i>j}\hat{J}_{ij}|c\rangle\rho_{cb}^{(n_p,n_t)}(t) - \langle c|\sum_{i>j}\hat{J}_{ij}|b\rangle\rho_{ac}^{(n_p,n_t)}(t)) + \\ &\left(\frac{\partial}{\partial t}\rho_{ab}^{(n_p,n_t)}(t)\right)_{|rad} - \sum_{c,d}(\Gamma_{bddc}\rho_{ac}^{(n_p,n_t)} + \Gamma_{addc}\rho_{cb}^{(n_p,n_t)} - \\ &\{\Gamma_{cabd} + \Gamma_{dbac}\}\rho_{cd}^{(n_p,n_t)})\end{aligned} \tag{37}$$

In comparison to eq 25 there appear two major differences. First, there is a new term proportional to $n_p\Omega_p + n_t\Omega_t$, which establishes resonance conditions between the external field and the optical transitions in the system. Second, the interaction with the radiation field couples RDM expansion coefficients $\rho_{ab}^{(n_p,n_t)}$ with different values of n_p and n_t. Applying the rotating wave approximation, the interaction with the external pump and probe field now reads

$$\begin{aligned}\left(\frac{\partial}{\partial t}\rho_{ab}^{(n_p,n_t)}(t)\right)_{|rad} = &\frac{i}{\hbar}E_p^*(t)(\langle b+1|\sum_j\hat{\mu}_j|b\rangle\rho_{ab+1}^{(n_p-1,n_t)}(t) - \\ &\langle a|\sum_j\hat{\mu}_j|a-1\rangle\,\rho_{a-1b}^{(n_p-1,n_t)}(t)) + \frac{i}{\hbar}E_p(t)\,(\langle b-1|\sum_j\hat{\mu}_j|b\rangle\times \\ &\rho_{ab-1}^{(n_p+1,n_t)}(t) - \langle a|\sum_j\hat{\mu}_j|a+1\rangle\rho_{a+1b}^{(n_p+1,n_t)}(t)) + \frac{i}{\hbar}E_t^*(t)\times \\ &(\langle b+1|\sum_j\hat{\mu}_j|b\rangle\,\rho_{ab+1}^{(n_p,n_t-1)}(t) - \langle a|\sum_j\hat{\mu}_j|a-1\rangle\rho_{a-1b}^{(n_p,n_t-1)}(t)) + \\ &\frac{i}{\hbar}E_t(t)\,(\langle b-1|\sum_j\hat{\mu}_j|b\rangle\,\rho_{ab-1}^{(n_p,n+1)}(t) - \\ &\langle a|\sum_j\hat{\mu}_j|a+1\rangle\rho_{a+1b}^{(n_p,n+1)}(t))\end{aligned} \tag{38}$$

Here, for example, $a + 1$ means that the electronic quantum number of the single molecule j should rise to that of the next electronic state. (This is a result of the rotating wave approximation.) The concrete value of j is determined by the action of the particular dipole operator $\hat{\mu}_j$. If we are already in the highest state, then this contribution should vanish.

The indices n_p and n_t indicate the minimal order of the interaction with the external fields, i.e. to find $\rho_{ab}^{(0,1)}$ different from zero, the probe pulse has to act at least in first order. To get a nonlinear response, however, also the pump pulse will contribute in higher orders to $\rho_{ab}^{(0,1)}(t)$. Because we want to include the pump pulse to an arbitrary order, it seems that we have to solve an arbitrarily large system of differential equations.

This is not the case as we will see in the following. We introduce the electronic quantum numbers p_a and p_b for the two monomers of Chl*a* and Chl*b*, respectively, and assume the system to be in its electronic ground state before the external fields starts to act (i.e., $n_p = n_t = 0$, $p_a = p_b = q_a = q_b = g \equiv 0$). Then, after an infinitesimal time step dt we look how the RDM expansion elements are generated due to the action of the external fields. After carrying out this procedure many times within the rotating wave approximation for which an absorption (emission) of a photon is connected with an excitation (deexcitation) of the CHl one finds for every value of t (identify g, e, and f with 0, 1, 2, respectively)

$$n_p + n_t + (p_a + p_b) - (q_a + q_b) = 0 \tag{39}$$

Before we can make use of the found conservation law among the indices of the density matrix, we have to take notice of the influence from the remaining part of the equations of motion. The crucial points are the dipole−dipole interactions and the IC part of the system−reservoir coupling, whereas the rest is diagonal with respect to the electronic states and hence will not change eq 39. If we derive the terms resulting from the dipole−dipole coupling, we find that they will not change $p_a + p_b$ and $q_a + q_b$, although they are off-diagonal with respect to the electronic states. This behavior is originated by the related part of the Hamiltonian which conserves the number of excitations (Heitler−London approximation). For the dissipative part related to the IC process we also find that the differences $q_a - p_a$ and $q_b - p_b$ remain unchanged. Therefore, we can conclude that eq 39 is valid for the whole set of equations of motion of the RDM. We make use from eq 39 and express n_p as $n_p = (q_a + q_b) - n_t - (p_a + p_b)$. For the numerical propagation of the RDM expansion coefficients $\rho_{ab}^{(n_p,n_t)}$ we drop the index n_p, because it is defined via eq 38.

To summarize the advantages of the plane-wave expansion, we may state that this technique directly gives the desired part of the polarization which is measured in the experiment. Additionally the numerical propagation becomes much easier because the fast oscillating carrier waves are separated and only the envelopes of the external fields enter the equations of motion. The price one has to pay is that the number of equations is enlarged three times. But since the pulse is long compared to the optical period, this disadvantage is compensated for by the increased step-width of the numerical propagation of the RDM. We should also mention here that a procedure has been proposed in ref 24 which extracts the desired part of the polarization by propagating the density matrix many times with different phases of the external field. The propagation however includes the whole field and not only the envelopes. Therefore it would not be suitable to manage the big numerical effort involved here.

III. Numerical Results

In the following our model is used to achieve a detailed understanding of the intensity-dependent two-color pump−probe experiment on the light harvesting complex LHC-II of photosystem II.[1] Furthermore, we discuss the limits of perturbation theories. In the former work[7] the dimer model could be successfully applied to a Chl*a*−Chl*b* dimer of the LHC-II. We gave an explanation of the found subpicosecond and picosecond time constants in the low-intensity case, where exciton annihilation can be neglected. The essential results of these calculations were as follows: (a) The subpicosecond time constant observed in the experiment reflects the delocalization of the exciton wave function over both monomers, (b) in the picosecond time the excitons relax from the upper to the lower one-exciton eigenstates, and (c) the transition dipoles of the monomers are arranged "in line" rather than "like a sandwich". Furthermore, it was possible to fix the values of various parameters which enter our calculation. (For a detailed discussion of the parameter values and their limits, the reader should have a look at ref 7.) The frequencies of the two effective vibrational modes were estimated from temperature-dependent linear absorption and fluorescence experiments to $\hbar\omega_a = \hbar\omega_b = 40$ cm^{-1}(5 meV). Here, we take the same frequency for both monomers as well as for all three electronic states of the monomer. From the microscopic distances and the assumed in line geometry for the monomer dipole moments, we get $J = -13$ meV for the dipole−dipole interaction among S_1 excitons. The transition energies between the S_0 ground states and the first excited S_1 states of Chl*a* and Chl*b* were chosen in accordance with the linear absorption maxima of the LHC-II at 680 and 650 nm, respectively. These are also the two wavelengths which have been used in the two-color experiment of ref 1. Therefore, we take the same carrier frequencies in our simulation. We will consider intramolecular excited state absorption, as it is known for Chl's from the work of ref 12. For the energy of the higher excited S_n state, we take twice the energy of the S_1 state. The external field can excite the S_n state only from the S_1 state but not directly from the ground state. The ratio of the respective dipole moments $m = |\mathbf{d}_j(f, e)|/|\mathbf{d}_j(e, g)|$ will be a fit parameter in our simulation, and we take it independent of monomer j. Besides m, the damping parameter $\hbar G^{(IVR)}$ (see its definition in ref 7) of the effective modes X_j could be estimated from the simulation of the low-intensity spectra.[7] For higher intensities where the occupation of the higher exciton manifolds and therefore IC becomes important, we will determine the IC coupling constant $\hbar k^{(IC)}$ (see eq 33). For the envelopes of the external pump and probe pulse we take a Gaussian shape of width 100 fs as in the experiment. The differential absorption measured in a pump−probe setup is given as

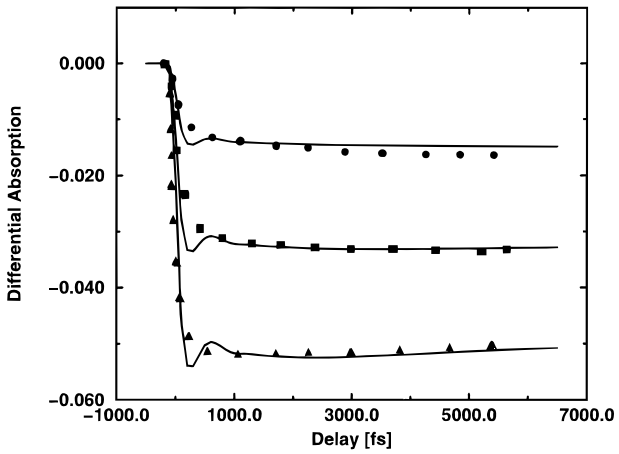

Figure 2. Two-color 100 fs pump−probe signals measured by ref 1 versus delay time for three different peak intensities of the pump beam. $I_0 = 6 \times 10^{13}$ photons cm^{-2} pulse^{-1} (circles), 2.2 I_0 (squares), and 3.1 I_0 (triangles). The drawn curves are the result of the simulations with the same increase of the intensity as in the experiment.

$$\frac{\Delta\alpha}{\alpha_0} = \frac{S_{\text{tot.}}(E_p, E_t, \tau) - S_{\text{tot.}}(E_p{=}0, E_t)}{S_{\text{tot.}}(E_p{=}0, E_t)} \tag{40}$$

where τ is the decay between the two pulses.

A. Intensity Dependent Differential Absorption. In Figure 2 we show $\Delta\alpha/\alpha_0$ for three different pump intensities in comparison with the experiment. The numerical results have been obtained in taking the following parameters: (a) ratio of the two transition dipole moments within a single Chl $m = 1.19$, (b) coupling strengths to the protein environment (introducing vibrational relaxation of the coordinates X_j) $\hbar G^{VR} = 0.1$ meV, and (c) internal conversion $\hbar k^{IC} = 0.3$ meV ($1/k^{IC} = 2.2$ ps).

An additional fit by changing the pump intensity independently was not necessary. Starting with a value of $I_0 = 6 \times 10^{13}$ photons cm^{-2} pulse^{-1}, it has been increased in accordance with the experiment by the factors 2.2 and 3.1, respectively (from the upper to the lower curve in Figure 2).

Both the femtosecond and the picosecond component are well-reproduced within our model. Since the former has been discussed in detail in our previous work,[7] we will focus here on the picosecond component of the signal. One can see that the signal falls for low pump intensities, whereas it rises at higher intensities. We stress that this qualitative change of the differential absorption cannot be understood within the commonly applied $\chi^{(3)}$ theory for which the signal should only scale linearly with intensity.

To get a deeper understanding of the involved physics, we calculate the occupation probability of the exciton eigenstates $|n\phi\rangle$

$$P_{n\phi}(X_a, X_b) = \sum_{\mathbf{pq}} c_p^{*(n\phi)}(X_a, X_b)\, \rho_{\mathbf{pq}}(X_a, X_b)\, c_{\mathbf{q}}^{(n\phi)}(X_a, X_b) \tag{41}$$

where the internal number ϕ counts the eigenstate in the n-exciton manifold ($n = 0...4$, $\mathbf{p} = \{p_a, p_b\}$, and $\mathbf{q} = \{q_a, q_b\}$ are the electronic quantum numbers of the dimer). The coefficients c_p^* and $c_{\mathbf{q}}$ are obtained by diagonalizing the electronic part of the Hamiltonian, including the dipole−dipole interaction (see eq 11 with $E = 0$) but using the effective vibrational coordinates X_a and X_b as classical quantities. We obtain exciton eigenstates for fixed values of X_a and X_b. It can be proven numerically that for the chosen system parameters

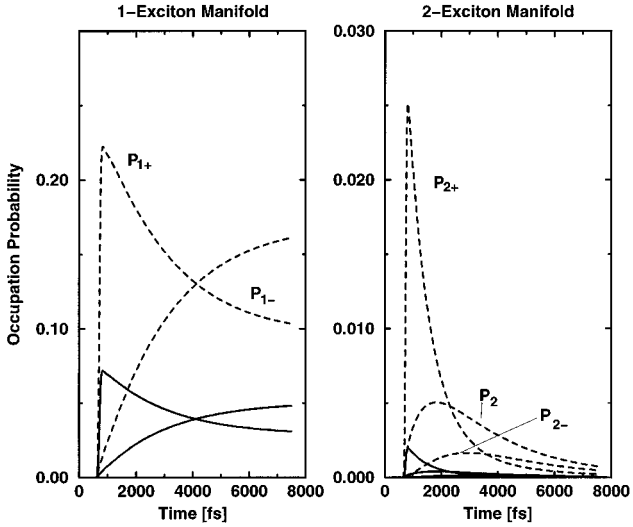

Figure 3. Multiexciton state population for the two extreme pump intensities $I_0 = 6 \times 10^{13}$ photons cm^{-2} pulse^{-1} (full line) and $3.1I_0$ (dashed line) versus time.

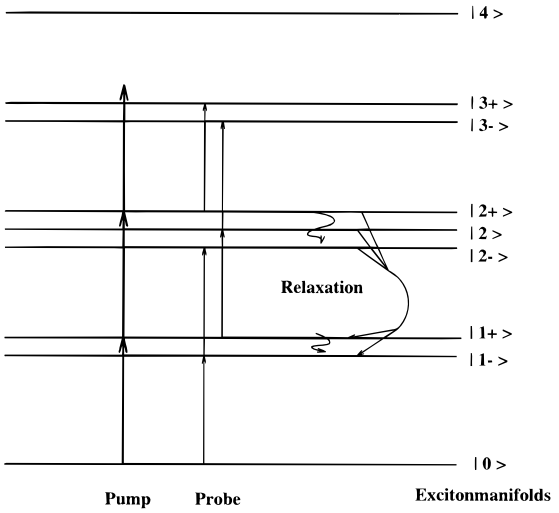

Figure 4. Electronic eigenstates of the dimer. Arrows indicate the action of the external fields in the two-color pump−probe setup. Wavy lines show the relevant relaxation processes within and between the exciton manifolds.

the dependence of $P_{n\phi}$ on X_a and X_b is rather weak ($\delta P_{n\phi}/P_{n\phi} < 0.01$). Therefore, we will not mention the distinct value of the vibrational coordinates at which the occupation probability has been calculated.

In Figure 3 we show the state occupation probabilities in the one- and two-exciton manifolds for the two extreme intensities I_0 (full line) and $3.1I_0$ (dashed line). To get an explanation of the obtained dynamics, the excitation conditions and relevant relaxation channels are shown in Figure 4. The high energetic pump pulse populates mainly the upper one-exciton state $|1+\rangle$ and the high upper two-exciton state $|2+\rangle$. Due to the interplay of the dipole−dipole coupling and the vibrational energy dissipation, we get a relaxation between exciton states in the same manifold (for example, the transition from $|1+\rangle$ to $|1-\rangle$). However, according to the interplay of the dipole−dipole interaction and IC there is also a relaxation between different exciton manifolds. Of course this becomes important at higher intensities when higher manifolds are populated. At low intensities the population of the one-exciton manifold will determine the nonlinear optical response. Due to the relaxation $|1+\rangle \rightarrow |1-\rangle$ there is an increase of the probe pulse transmission as a consequence of stimulated emission from the low energetic

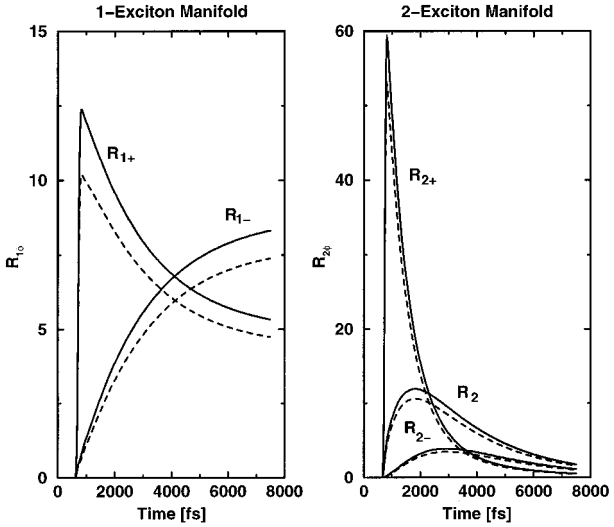

Figure 5. Multiexciton state population in terms of powers of the pump-beam intensity versus time for the two intensities I_0 (full line) and $3.1I_0$ (dashed line). As explained in the text the $P_{n\phi}$'s give the occupation of the *eigenstates* ϕ in the n th exciton manifold. Here we show the occupations within the first two manifolds (i.e., $n = 1, 2$).

one-exciton state to the ground state. But, at higher intensities this effect is overcompensated for by an increase of the probe pulse absorption. This originates from the relaxation between the two- and the one-exciton manifolds which opens new channels for the probe pulse to be absorbed. Additionally, Figure 3 displays that the ratio between the occupations of the two- and the one-exciton manifolds becomes larger with increasing intensity. This causes the qualitative change of the differential absorption in the related pump−probe experinment.

One aspect concerning the absolute value of the intensity I_0 should be mentioned now. Since the dipole strengths of the pigments within the protein environment of the LHC-II as well as the relative dielectric constant ϵ_r of the medium are not very exactly known, we used the product of the external field and the dipole-moment (compare eq 38) as a fit parameter too. The envelope of the external field $E(t)$ and its intensity I in the above given units are related via $I = \epsilon_r^{1/2} c/(2\pi\hbar\Omega) \int_{-\infty}^{+\infty} dt\, |E(t)|^2$, with c being the velocity of light. Therefore from the comparison of the experimental value of I_0 and the theoretical fit, we can give an estimation for the effective monomer $S_0 \rightarrow S_1$ transition dipole strengths μ_{eff}. For Chl*b* we get $\mu_{\text{eff}}^{(b)} = 2.7$ Debye, whereas for Chl*a* we used a 1.2 times higher value. Although the true values of the dipole strengths are supposed to lie a little bit higher (between 3 and 4 D) our estimates give the right order for them, what can be understood as a nice proof of our theory.

B. Test of Perturbation Theories. In the following we want to verify our qualitative statement concerning the validity of the perturbation theory (with respect to the radiation field) for the simulation of the pump−probe experiment. For this reason we use the fact that within $\chi^{(3)}$ theory the population of the one-exciton states should scale linearly with intensity and within $\chi^{(5)}$ theory the population of the two-exciton states should scale with the second power of intensity. Therefore we define the ratio

$$R_{n\phi} = P_{n\phi}/I^n \tag{42}$$

of the occupation probability and the nth power of pump intensity. In Figure 5 the quantities $R_{n\phi}$ are shown for the two extreme intensities I_0 (full line) and $3.1I_0$ (dashed line). One can clearly see that the deviations from $\chi^{(3)}$ theory are larger than those from $\chi^{(5)}$ theory. At higher intensities, of course,

the deviations from perturbation theory get much bigger (not shown here). For the largest value of the experimental intensities we are at the point were $\chi^{(3)}$ theory becomes invalid, although there is only an error of about 10% in the occupation probabilities of the one-exciton states (estimated from the difference between the full and dashed lines in Figure 5). Otherwise, the pump−probe signal should not rise on a picosecond time scale but fall like that at low intensities. Obviously, the intensity has reached a value where nonlinearities in the differential absorption become important.

IV. Conclusions

Using a heterodimer model including a Chl*a* and a Chl*b* molecule ultrafast spectroscopic findings of ref 1 on the LHC-II of higher plants could be well-reproduced. Since the structure of this pigment−protein complex is known with a resolution of 3.4 Å, only a restricted number of fit parameters enters our calculations. We need the spectral density of the protein vibrations at a special frequency, the transition dipole moment for the transition from the first excited singlet state to the higher one, and the IC rate for the reverse process. The frequencies of the effective protein coordinates which have been handled quantum mechanically have not to been newly determined. We could take the value already used in former calculations. It was only necessary to adjust the potential energy surface of the higher excited singlet state in a manner in which agreement with the experimental findings is achieved. We consider it as a main advantage of our model that no separate fit of the intensity was necessary to reproduce the intensity dependence of the differential absorption. Getting coincidence with the measured signal at low pump intensity, we increased the intensity in the same manner as in the experiment and obtained a nice agreement also at higher values of the pump intensity.

Although the heterodimer model used does not give a complete description of the LHC-II pigment−protein complex, an acceptable agreement of our calculations with the measured data could be achieved. This is the case for the one-color as well as the two-color experiment. It was also possible to demonstrate that the nonperturbative inclusion of the light field should be appropriate for the pump intensities used in the experiment. A notable deviation from an approach based on the nonlinear susceptibility of third order ($\chi^{(3)}$ theory) and a weaker deviation from a $\chi^{(5)}$ theory have been obtained.

Finally, we have to note that a treatment of the dimer in an approach without the inclusion of the quantum dynamics of selected effective protein coordinates would give worse results for the simulation of the intensity dependent two-color pump−probe experiments[25] as well as for the low-intensity one-color pump−probe simulation.[26] We interpret this result as the presence of some retardation effects in the exciton vibrational coupling. In the description with the effective modes this retardation follows by the motion of the wave packet related to the effective vibrational coordinates. Alternatively, one can understand this retardation as a hint that the description of the exciton reservoir interaction should include some non-Markovian effects.

Finishing the whole discussion, we would like to state that one should consider the present results as reference data which allow checking of more crude calculations which are necessary if one goes beyond the dimer model and tries to simulate a collection of some ten of Chl molecules.

Acknowledgment. Financial support by the *Deutsche Forschungsgemeinschaft* through Grant Ma 1356/1-2 as well as by the *European Science Foundation* is gratefully acknowledged. T.R. is thankful for the financial support by the *Studienstiftung des Deutschen Volkes*.

References and Notes

(1) Bittner, T.; Irrgang, K.-D.; Renger, G.; Wasielewski, M. R. *J. Phys. Chem.* **1994**, *98*, 11821.

(2) McDermott, G.; Prince, S. M.; Freer, A. A.; Hawthornthwaite-Lawless, A. M.; Papiz, M. Z.; Cogdell, R. J.; Isaacs, N. W. *Nature* **1995**, *374*, 517.

(3) van Grondelle, R.; Dekker, J. P.; Gillbro, T.; Sundström, V. *Biochim. Biophys. Acta* **1994**, *1187*, 1.

(4) Kühlbrandt, W.; Wang, D. N.; Fujiyoshi, Y. *Nature* **1994**, *367*, 614.

(5) Kühn, O.; Renger, Th.; May, V. *Chem. Phys.* **1996**, *204*, 99.

(6) Renger, Th.; Voigt, J.; May, V.; Kühn, O. In *Femtochemistry-Ultrafast Chemical and Physical Processes in Molecular Systems, Proceedings of the Lausanne; Conference*; Chergui, M., Ed.; World Scientific, Singapore: 1996; p 401.

(7) Renger, Th.; Voigt, J.; May, V.; Kühn, O. *J. Phys. Chem.* **1996**, *100*, 15654.

(8) Renger, Th.; Voigt, J.; May, V.; Kühn, O. In *Proceedings of the Conference Excitonic Processes in Condensed Matter*; Schreiber, M., Ed.; Dresden University Press: Dresden, Germany, 1996; p 279.

(9) Kenkre, V. M.; Reineker, P. In *Exciton Dynamics in Molecular Crystals and Aggregates*; Springer Tracts in Modern Physics; Springer: Berlin, 1982; Vol. 94.

(10) *Excitons*; Rashba, E. J., Sturge, M. D., Eds.; North-Holland: Amsterdam, 1982.

(11) Agranovich, V. M.; Galanin, M. D. Electronic Excitation Energy Transfer in Condensed Matter. In *Modern Problems in Condensed Matter Sciences*; North-Holland: Amsterdam, 1983; Vol. 4.

(12) Shepanski, J. F.; Anderson, R. W. *Chem. Phys. Lett.* **1981**, *78*, 165.

(13) Mukamel, S. *Principles of Nonlinear Optical Spectroscopy*; Oxford University Press: New York, 1995.

(14) Chachisvilis, M.; Pullerits, T.; Jones, M. R.; Hunter, C. N.; Sundström, V. *Chem. Phys. Lett.* **1994**, *224*, 345.

(15) Chachisvilis, M. Electronic and vibrational coherence in photosynthetic and model systems. Ph.D. Thesis, Lund University, 1996.

(16) Vos, M. H.; Rappaport, F.; Lambry, J. C.; Breton, J.; Martin, J. L. *Nature* **1993**, *363*, 320.

(17) Vos, M. H.; Jones, M. R.; Hunter, C. N.; Breton, J.; Martin, J. L. *Proc. Natl. Acad. Sci. U.S.A.* **1994**, *91*, 12701.

(18) Voigt, J.; Maciy, K.; Schrötter, T. *Photosynthetica* **1994**, *30*, 603.

(19) Spano, F. C. *Phys. Rev. Lett.* **1991**, *67*, 3424.

(20) Knoester, J.; Spano, F. C. *Phys. Rev. Lett.* **1995**, *74*, 2780.

(21) Chernyak, V.; Mukamel, S. *J. Opt. Soc. Am. B* **1996**, *13*, 1302.

(22) Kühn, O.; Mukamel, S. *J. Phys. Chem. B* **1997**, *101*, 809.

(23) Kühn, O.; May, V.; Schreiber, M. *J. Chem. Phys.* **1994**, *101*, 10404.

(24) Seidner, L.; Stock, G.; Domcke, W. *J. Chem. Phys.* **1995**, *103*, 3998.

(25) Renger, Th.; May, V. *Phys. Rev. Lett.* **1997**, *78*, 3406.

(26) Renger, Th.; May, V. *Photochem. Photobiol.*, submitted, for publication.